Geomechanics and Engineering, *Vol. 32, No. 3 (2023) 321-333*
https://doi.org/10.12989/gae.2023.32.3.321

Influence of size and location of a pre-existing fracture on hydraulic fracture propagation path

Bo Zhang[1,2a], Yao Li[1b], Xue Y. Yang[3c], Shu C. Li[4d], Chao Wei*[4,5] and Juan Songa**[1]

[1]*School of Civil Engineering, Shandong University, Jinan, Shandong 250061, PR China*
[2]*Structural Laboratory, Shandong Institute of Transportation Science, Jinan, Shandong 250014, PR China*
[3]*Shandong Urban Construction Vocational College, Jinan, Shandong 250014, PR China*
[4]*Research Center of Geotechnical and Structural Engineering, Shandong University, Jinan, Shandong 250061, PR China*
[5]*State Key Laboratory for Geomechanics and Deep Underground Engineering, China University of Mining and Technology, Xuzhou, Jiangsu 221116, China*

(*Received Januaryr 11, 2022, Revised January 10, 2023, Accepted January 17, 2023*)

Abstract. Rock masses often contain natural fractures of varying sizes, and the size of the natural fractures may affect the propagation of hydraulic fractures. We conduct a series of triaxial hydraulic fracturing tests to investigate the effect of the pre-existing fracture size *a* on hydraulic fracture propagation. Experimental results show that the pre-existing fracture size impacts hydraulic fracture propagation. As the pre-existing fracture size increases, the hydraulic fracture propagates towards the pre-existing fracture tips, evidenced by the decreased distance between the final hydraulic fracture and the pre-existing fracture tips. Furthermore, the attracting effect of pre-existing fracture tips increases when the distance between the wellbore and the pre-existing fracture is short (L/D=2 or 4 in this study). With increased distance between the wellbore and the pre-existing fracture (L/D=6 in this study), the hydraulic fracture propagates to the middle of the pre-existing fracture rather than the tips, as the attracting effect of the pre-existing fracture diminishes.

Keywords: elastic strain energy density; fracture propagation; fracture propagation path; hydraulic fracturing; pre-existing fracture size

1. Introduction

Hydraulic fracturing has been widely used in the oil and gas industry to extract hydrocarbons from both conventional and unconventional reservoirs. Reservoirs, especially unconventional reservoirs, often contain natural fractures that can affect the propagation paths of hydraulic fractures. The interaction between hydraulic and natural fractures during fracturing operations is one of the key factors impacting the generation and the final geometry of fracture network. Such interaction is often influenced by the size, location, and orientation of natural fractures. Therefore, it is of significance to investigate the interaction between hydraulic fractures and natural fractures for production improvement.

Many scholars have studied hydraulic fracture propagation under different conditions. For example, confining stress significantly impacts hydraulic fracture initiation and propagation behavior, and the ratio between fracture initiation pressure and confining stress is small under high confining stress (Bohloli *et al.* 2006, Mao *et al.* 2017, Ham *et al.* 2019). In addition, the larger the horizontal stress difference, the greater the curvature of the hydraulic fracture. The effect of heterogeneity during hydraulic fracture propagation is also examined, and the larger the proppant particles are in the fractures, the more complex the hydraulic fractures become (Ma *et al.* 2017, Jiang *et al.* 2018).

Pre-existing fractures have a significant impact on the propagation path of hydraulic fractures, which is affected by the competition between weak surfaces and stress effects. Some scholars have studied the morphology of pre-existing and hydraulic fractures (Salam *et al.* 2017, Dehghan *et al.* 2015, Jang *et al.* 2015). Using samples containing pre-existing fractures, they found that the arrested area increases with increasing shear strength of the pre-existing fracture. Under high horizontal stress difference, the strike direction of the pre-existing fracture has a larger impact than the dip direction on the hydraulic fracture during fracture propagation (Dehghan *et al.* 2015). Fracture propagation modes are explored through experiments and the geometric morphology of hydraulic fractures is summarized (Tan *et al.* 2017, Hou *et al.* 2018). Furthermore, researchers have studied the conditions for the formation of hydraulic fracture networks, and found that complex fracture networks are generally formed by the connections between hydraulic fractures and natural fractures

*Corresponding author, Ph.D.
E-mail: 392470762@qq.com
**Corresponding author. Ph.D.
E-mail: songjuan@sdu.edu.cn
[a]Professor
E-mail: zhangbo1977@sdu.edu.cn
[b]Ms.
E-mail: 2806151685@qq.com
[c]Ph.D.
E-mail: 274679821@qq.om
[d]Professor
E-mail: lishucai@sdu.edu.cn

ISSN: 2005-307X (Print), 2092-6219 (Online)

Table 1 Physico-mechanical parameters of cement mortar

	Young's modulus E (GPa)	Compressive strength σ_c (MPa)	Tensile strength σ_t (MPa)	Poisson's ratio μ	Fracture toughness K_{IC} ($MPa \cdot m^{1/2}$)
Cement mortar	0.302	22.26	0.88	0.2	0.51

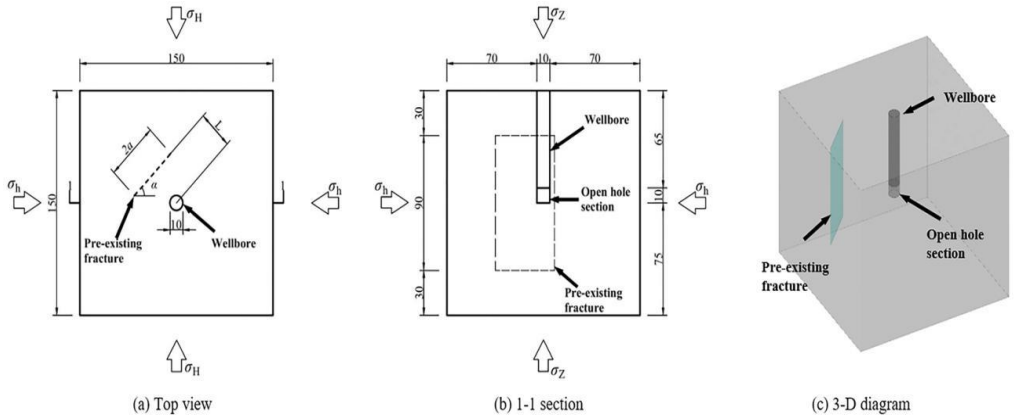

Fig. 1 Schematics for the testing specimens

or bedding planes (Yan *et al.* 2019). In addition, branches or deviations of hydraulic fractures are also beneficial to the creation of complex fracture networks. Moreover, the interaction between hydraulic fractures and natural fractures is also affected by the difference in two confining stresses (i.e., horizontal stresses). Specifically, the greater the stress difference, the less complex the fracture network (Fan *et al.* 2014, Warpinski *et al.* 1984, Guo *et al.* 2014, Hadei *et al.* 2021). Hydraulic fracture deflection criterion is theoretically investigated and a low friction coefficient between fracture surfaces is more favorable for hydraulic fracturing (Zeng *et al.* 2017). The impact of the distance between the pre-existing fracture and the wellbore on hydraulic fracture propagation is studied, and when the pre-existing fracture is close to the wellbore, the hydraulic fracture propagates to the tip of the pre-existing fracture (Zhang *et al.* 2018). On the other hand, when the pre-existing fracture is far away from the wellbore, the influence of the pre-existing fracture tip on the hydraulic fracture propagation diminishes. The propagation behavior of hydraulic fractures approaching pre-existing fractures is closely related to the distribution pattern of pre-existing fractures. Hydraulic fractures passing through natural fractures is examined from both theoretical and experimental perspectives (Zhao *et al.* 2019, Liu *et al.* 2014, Taleghan *et al.* 2016). In summary, pre-existing fractures affect the propagation path of hydraulic fractures and the ultimate fracture network. However, the interaction between hydraulic fractures and pre-existing fractures of different sizes has not been fully investigated.

Numerical simulation methods have been widely used in studying hydraulic fracturing and the effects of anisotropy, interface frictional strength, fluid viscosity, and pre-existing fractures on fracture propagation (Nadimi *et al.* 2016, Al-Rubaie *et al.* 2020, Behnia *et al.* 2015, Wei *et al.* 2021). Luo *et al.* (2018) established a seepage-stress coupling model based on the Extended Finite Element Method (XFEM) and found that it is easier for a hydraulic fracture to cross a natural fracture and continue to propagate if they are orthogonal, and the hydraulic fracture is more likely to be arrested by an oblique natural fracture. Kwok *et al.* (2020) used the discrete element method to study the hydraulic fracturing process and showed that sedimentary beddings and pre-existing joints have a significant impact on the hydraulic fracture propagation. Rock heterogeneity increases the stress shadowing effect, and the increase of stress anisotropy can offset the stress shadowing effect. In this work, we use the finite element method to develop an energy model for hydraulic fracture propagation and explore the hydraulic fracture propagation path. Furthermore, we use the extended finite element method to simulate the hydraulic fracture propagation with the presence of a pre-existing fracture under different conditions.

Previous studies have investigated the impact of the distance between the wellbore and the pre-existing fracture on hydraulic fracture propagation. When the pre-existing fracture is close to the wellbore, the hydraulic fracture propagates to the pre-existing fracture tip. When the pre-existing fracture is located far from the wellbore, the impact of the pre-existing fracture tips on the propagating hydraulic fracture is reduced (Zhang *et al.* 2018). However, the impact of the size and location of the pre-existing fracture on hydraulic fracture propagation has not been fully investigated. In this study, we conduct laboratory experiments to explore such impact.

2. Hydraulic fracturing experiment

In this work, we conducted laboratory experiments on specimens made of cement mortar, consisting of water, dry sand with particle size smaller than 1.25 mm, and 325# cement. The mass ratio of the three materials is 0.65:3.5:1.

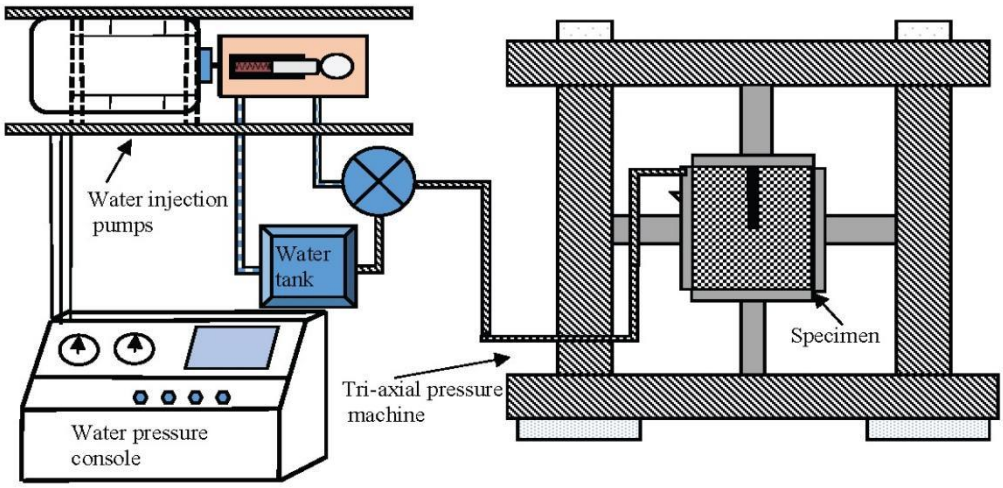

Fig. 2 Hydraulic fracturing experiment apparatus

Table 2 Experimental conditions

Group	Testing specimens	The ratio of maximum to minimum horizontal stressm(σ_H: σ_h)	The maximum and minimum horizontal stresses (σ_H: σ_h)/MPa	vertical stress σ_z/*MPa*	Pre-existing fracture and vertical wellbore center spacing *L*/*mm*	Pre-existing fracture width 2a/mm
1	1-1#	1	2.667 : 2.667	3.56	20	40
	1-2#					60
	1-3#					80
	1-4#	2	2.667 : 1.3335			40
	1-5#					60
	1-6#					80
2	2-1#	1	2.667 : 2.667	3.56	40	40
	2-2#					60
	2-3#					80
	2-4#	2	2.667 : 1.3335			40
	2-5#					60
	2-6#					80
3	3-1#	1	2.667 : 2.667	3.56	60	40
	3-2#					60
	3-3#					80
	3-4#	2	2.667 : 1.3335			40
	3-5#					60
	3-6#					80

The physico-mechanical properties of the rock-like materials are listed in Table 1. The specimen size is 150 mm × 150 mm × 150 mm. The material use to represent natural fractures is a rectangular piece of paper in three sizes, which are 90 mm × 40 mm × 0.5 mm, 90 mm × 60 mm × 0.5 mm, and 90 mm × 80 mm × 0.5 mm (Height × Width × Thickness).

We used the following procedure to prepare the testing specimens. (1) Use a standard size sieve to obtain sand with particles smaller than 1.25 mm. (2) Fix the paper that mimics the natural fracture through thin lines in the cubic mold. (3) Pour the weighted water, cement, and sand into the blender and mix evenly to prepare the cement mortar.

(4) Pour the prepared cement mortar into the mold treated by step (2), place the mold with cement mortar on the vibration table, and vibrate at room temperature until no more bubbles appear from the surface of the cement mortar. (5) After 12 hours, remove the cement mortar specimen from the mold and place it in a curing box for 28 days with a relative humidity greater than 95%, and a temperature of 20±1.5℃.

After the curing process is completed, a circular hole with a length of 75 mm is inserted into the center from the upper surface of the specimen and a metal tube with a wall thickness of 1 mm is placed in the hole to mimic the vertical

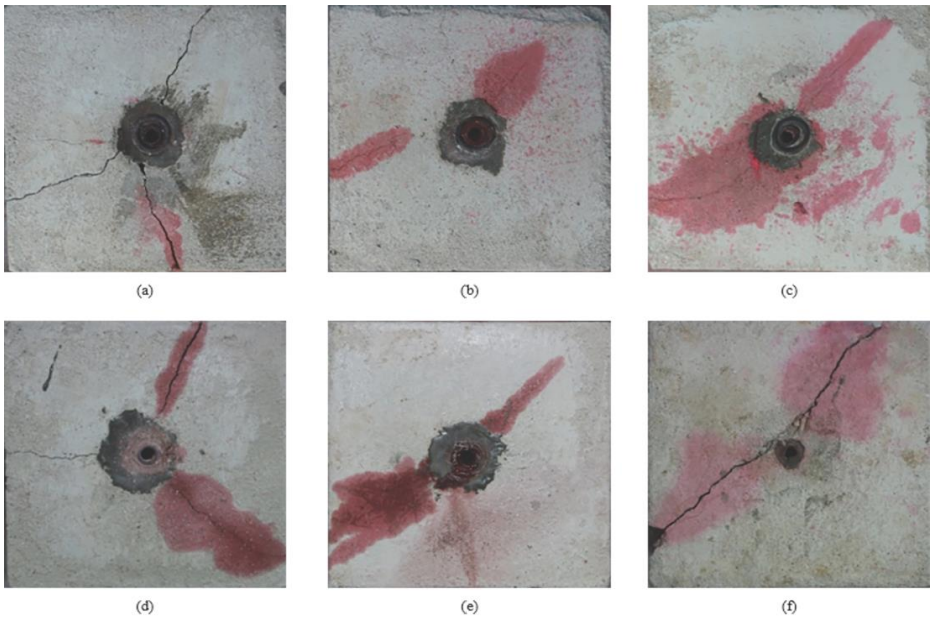

Fig. 3 Experimental results of hydraulic fracture propagation in Group 1: (a)-(f) is testing specimens 1-1#-1-6#

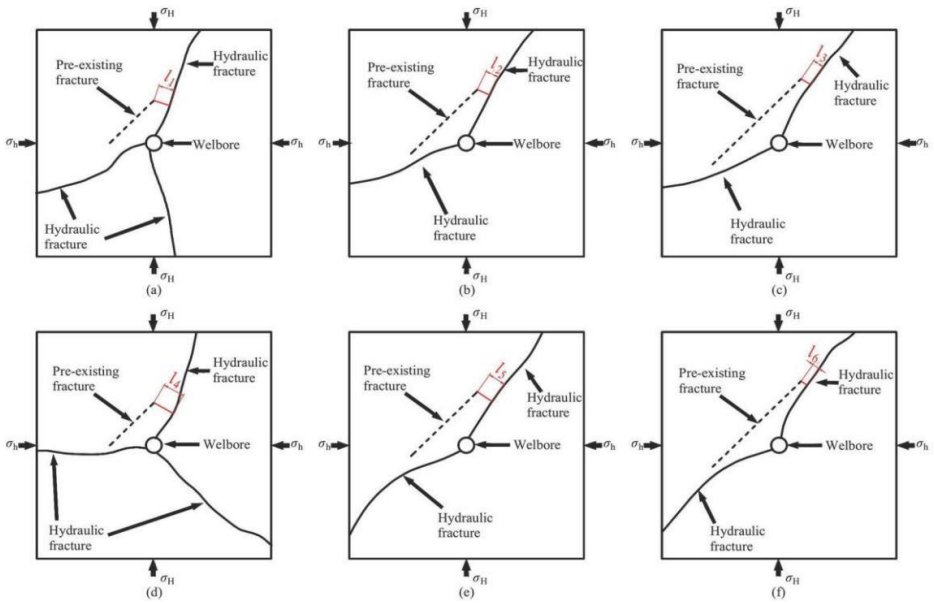

Fig. 4 Schematic of hydraulic fracture propagation in Group 1: (a)-(f) is the specimens 1-1#-1-6#

wellbore, and a 10 mm long open hole section is left. After the high-pressure water is injected to the specimen, a hydraulic fracture will initiate and propagate in the open hole section. In this work, the angle between the pre-existing fracture and the horizontal direction is 45°, as illustrated in Fig. 1.

Fig. 2 shows the apparatus used in this experiment that consists of a hydraulic pressure supply device and a triaxial loading device. The hydraulic pressure supply device is set up as a constant flow rate condition with a injection rate of 0.24 L/min. First, the specimen is placed in the triaxial loading device, and then the three principal stresses σ_H, σ_h, σ_z are applied to the designed values. After that, the fracturing fluid (water in this case) is injected into the wellbore through the hydraulic pressure supply device until the specimen is hydraulically fractured.

This experimental study is divided into three groups, each containing two confining stress ratios and three different sizes of the pre-existing fracture. The experimental conditions are listed in Table 2.

3. Experimental results

It can be seen from Figs. 3-8 that the propagation of hydraulic fractures is affected by the size of the pre-existing fracture and the distance between the wellbore and the pre-existing fracture.

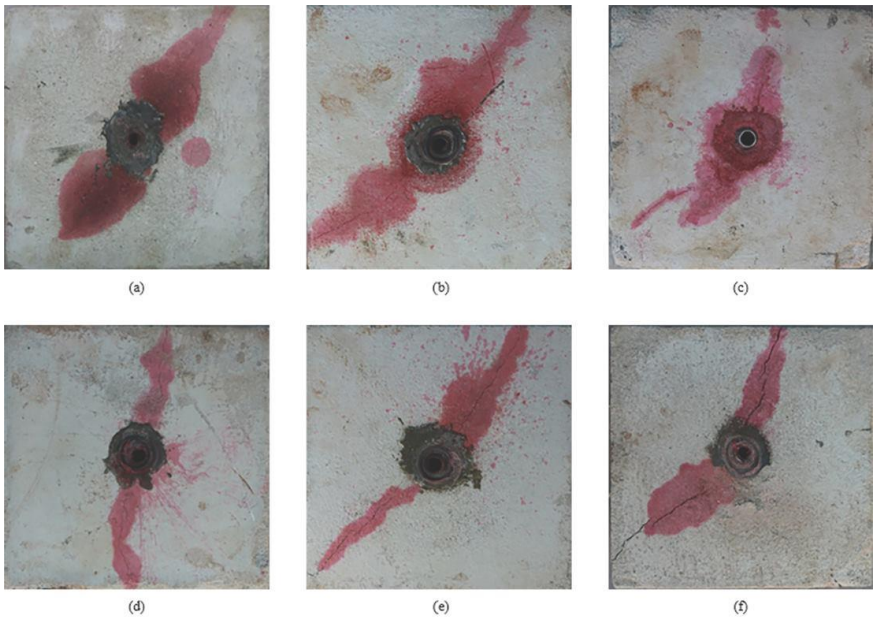

Fig. 5 Experimental results of hydraulic fracture propagation in Group 2: (a)-(f) is testing specimens 2-1#-2-6#

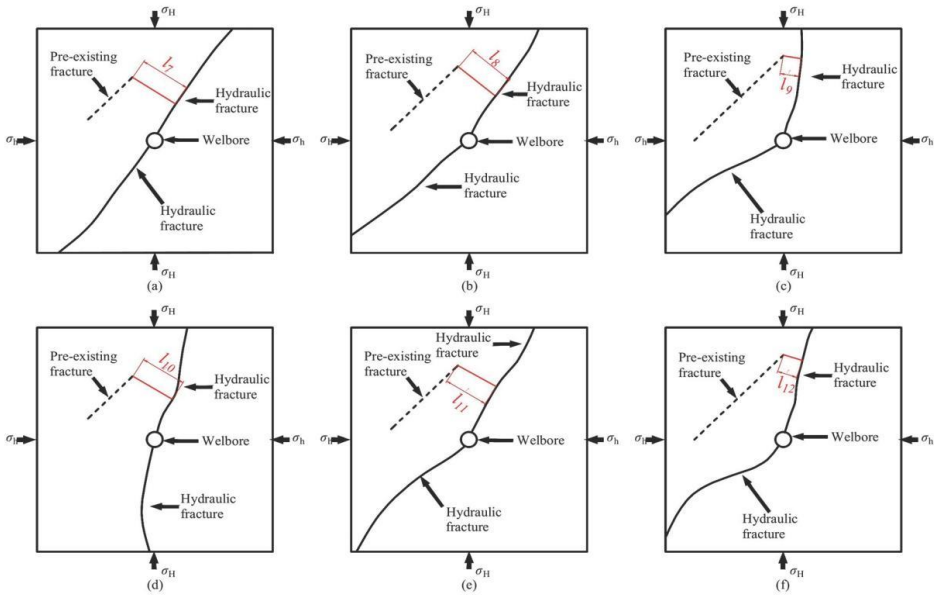

Fig. 6 Schematic of hydraulic fracture propagation in Group 2: (a)-(f) is testing specimens 2-1#-2-6#

Figs. 3-6 show that the distance *l* between the pre-existing fracture tips and the hydraulic fracture varies with changing pre-existing fracture size. With increasing pre-existing fracture size, the distance l decreases (l1>l2>l3, l4>l5>l6; l7>l8>l9, l10>l11>l12), indicating that as the pre-existing fracture size increases, so does the attracting ability from the pre-existing fracture to the hydraulic fracture.

Fig. 9 shows the hydraulic fracture propagation paths from specimens 1-1# and 1-3#, from which we find that the pre-existing fracture profile in specimen 1-3# (Fig. 9(b)) is more evident than that in specimen 1-1# (Fig. 9(a)). Specifically, the hydraulic fracture in specimen 1-3# is closer to the pre-existing fracture tip than the one in specimen 1-1#. The closer distance implies that the pre-existing fracture tip in specimen 1-3# has a stronger attraction on the hydraulic fracture than that in specimen 1-1#. This result indicates that the larger the pre-existing fracture, the stronger the attracting ability the pre-existing fracture tips have on hydraulic fracture propagation.

The distance between the wellbore and the pre-existing fracture of Group 1 specimens (1-1#, 1-2#, and 1-3#) is shorter than that of Group 2 specimens (2-1#, 2-2#, and 2-3#). Figs. 3-6 show that the distance l between the hydraulic fracture and the pre-existing fracture tip is longer in Group 2 than that in Group 1. For example, l1 in specimen 1-1# is shorter than l7 in specimen 2-1#. This indicates that the attracting ability of the pre-existing fracture tips of Group 2 specimens is smaller than that of Group 1 specimens.

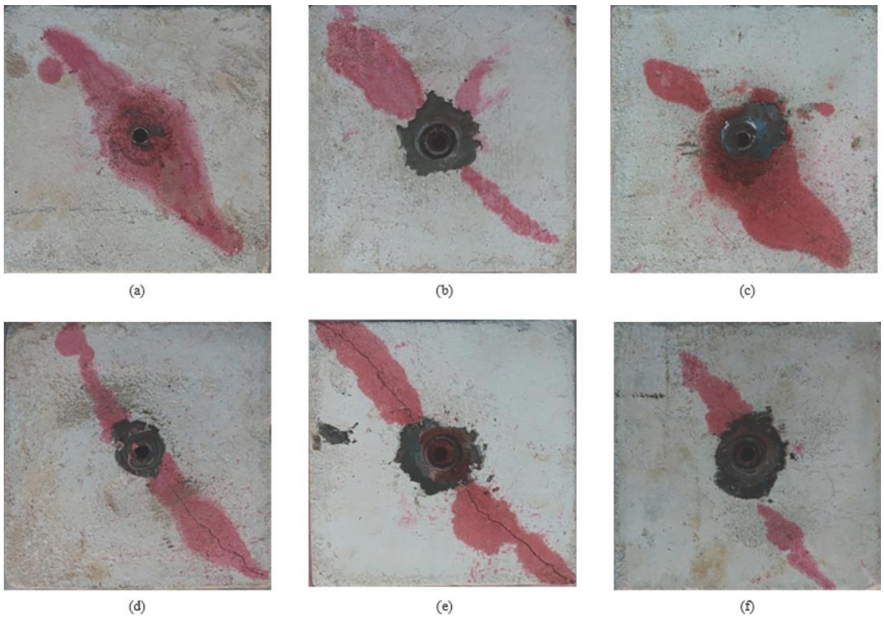

Fig. 7 Experimental results of hydraulic fracture propagation in Group 3: (a)-(f) is testing specimens 3-1#-3-6#

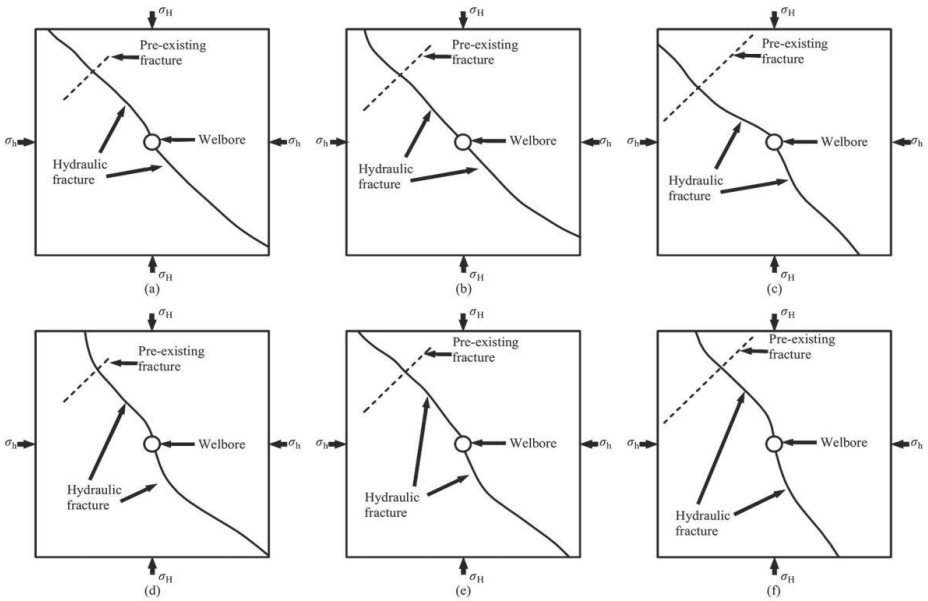

Fig. 8 Schematic of hydraulic fractures propagation in Group 3: (a)-(f) is testing specimens 3-1#-3-6#

The attracting ability decreases with increasing distance between the wellbore and the pre-existing fracture, and the influence of the pre-existing fracture size also reduces with distance. No pre-existing fracture appears on the hydraulic fracture surfaces, as shown in Fig. 10, indicating that the hydraulic fractures did not extend to the pre-existing fractures.

When L=60 mm (L/D=6), as the distance between the wellbore and the pre-existing fracture increases, the attraction tendency of the pre-existing fracture tips to hydraulic fractures is smaller than that of the pre-existing fracture with a shorter distance, and the pre-existing fracture tip does not attract the hydraulic fracture, and the effect of the pre-existing fracture size on hydraulic fracture propagation diminishes, as shown in Figs. 7 and 8. The hydraulic fracture propagates toward the middle of the pre-existing fracture, which implies that the pre-existing fracture tip has a very limited attracting ability to the hydraulic fracture. We recorded the breakdown pressures under different testing conditions. As the size of the pre-existing fracture near the wellbore increases, the breakdown pressure decreases gradually, and on the other hand, as the distance between the pre-existing fracture and the wellbore increases, the breakdown pressure increases, as provided in Table 3.

During hydraulic fracturing experiments, we use an acoustic emission system to monitor the acoustic emission signals when the hydraulic fracture initiates and propagates

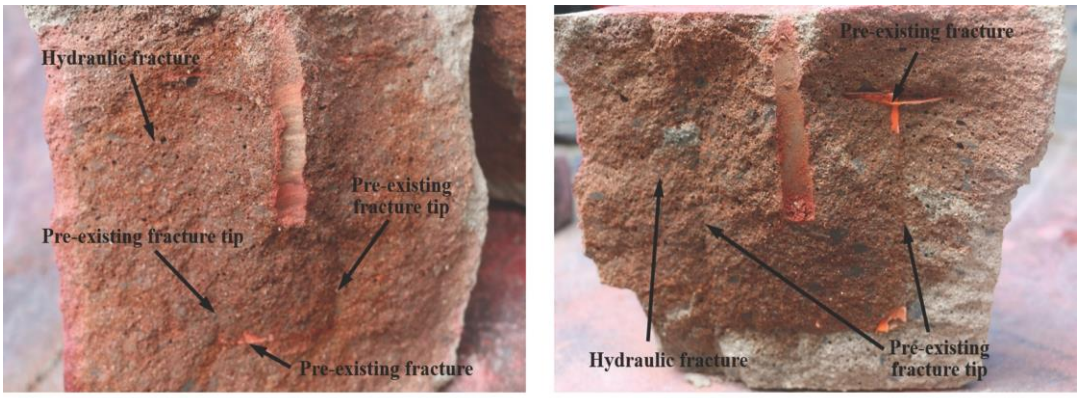

(a) testing specimen 1-1# (b) testing specimen 1-3#

Fig. 9 Hydraulic fracture propagation path of the testing specimens 1-1# and 1-3#

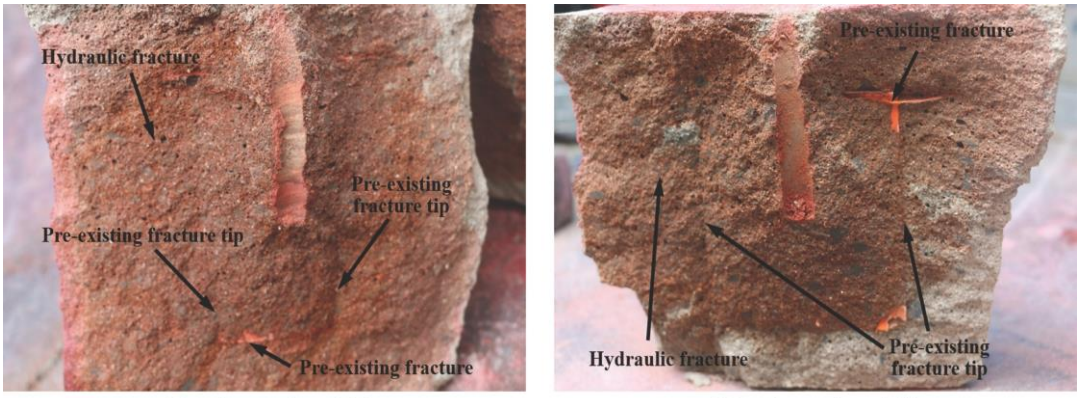

(a) testing specimen 1-1# (b) testing specimen 1-3#

Fig. 10 Hydraulic fracture propagation path of the testing specimens 1-1# and 1-3#

Table 3 Breakdown pressures under different test conditions

Group	Testing specimens	Pre-existing fracture width 2*a*/*mm*	Breakdown pressures/*MPa*
1	1-1#	40	8
	1-2#	60	7.7
	1-3#	80	7.5
	1-4#	40	7.5
	1-5#	60	7.5
	1-6#	80	6.8
2	2-1#	40	8.7
	2-2#	60	8.6
	2-3#	80	8.2
	2-4#	40	8.5
	2-5#	60	8.2
	2-6#	80	7.3
3	3-1#	40	9.6
	3-2#	60	9.2
	3-3#	80	9.1
	3-4#	40	9.4
	3-5#	60	9.5
	3-6#	80	8.5

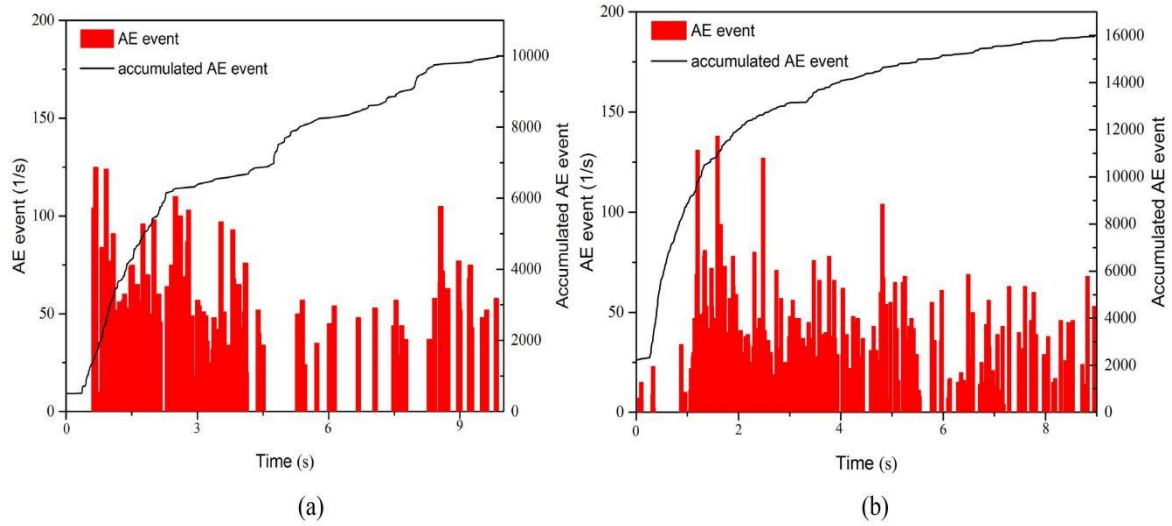

Fig. 11 Acoustic emission results of specimens: (a) 2-1# and (b) 2-3#

with different sizes of pre-existing fracture, which can reflect the damage and failure state of the specimen. Acoustic emission characteristics vary when hydraulic fractures initiate and propagate with the presence of pre-existing fractures of different sizes. We find that with the increase of the pre-existing fracture size, the breakdown pressure of the hydraulic fractures gradually is reduced, the peak signal of AE events is weakened, and the number of cumulative acoustic emission events is decreased, indicating that the degree of damage of specimens with longer pre-existing fractures is low, as shown in Fig. 11. During the initial loading stage, water pressure is low, so the specimen is compacted. Since there is no fracture in the compaction stage, acoustic emission events are very weak. As the injection pressure reaches the breakdown pressure, acoustic emission events rise rapidly to peak signals, and then the primary fracture is created in the specimen. Subsequently, water pressure decreases, the primary fracture propagates, and the acoustic emission event magnitudes are low again.

4. Numerical analysis

In order to better understand the effect of the pre-existing fracture size on hydraulic fracture propagation, we perform numerical simulation using the finite element software ABAQUS. We use the two-dimensional plane strain model to simulate the initiation and propagation of hydraulic fractures in the open hole section of the wellbore. The material properties of the model are: elastic modulus E of 302MPa and Poisson's ratio μ of 0.2. In the model, normal stress is applied at the boundaries according to the in-situ stress, and then the hydraulic pressure is applied. The wellbore pressure applied in the model is 10 MPa and the confining stress applied is 2.667 Mpa ($\sigma_H = \sigma_h = 2.667$ MPa). In the numerical model, the element type used for the pre-existing fracture tips is the 6-node quadratic plane strain triangle element, while the 8-node biquadratic plane strain quadrilateral element is used for the rest of the model. We use the strain energy model to reflect the energy characteristics of the interaction between hydraulic fractures and pre-existing fractures and use the extended finite element method to simulate the propagation of hydraulic fractures under different conditions.

The definition of strain energy density can be expressed as

$$U^e = \frac{1}{2}\sigma_1{\varepsilon_1}^2 + \frac{1}{2}\sigma_2{\varepsilon_2}^2 + \frac{1}{2}\sigma_3{\varepsilon_3}^2 \quad (1)$$

where U^e is the elastic strain energy released by the element, σ_1, σ_2, σ_3 are the stresses in three principal stress directions, and ε_1, ε_2, ε_3 are the elastic strain in three principal stress directions.

Specimens 1-1#, 1-2#, and 1-3# are simulated with the finite element method. In these three specimens, the distributions of elastic strain energy density in the model are shown in Fig. 12. By comparing the elastic strain energy density, it can be found that under the same loading condition, the elastic strain energy density at the pre-existing fracture tip areas increases with increasing pre-existing fracture size. In Figs. 12(a), 12(d) and 12(g), the pre-existing fracture lengths are 40 mm, 60 mm, and 80 mm, and the maximum elastic strain energy densities at pre-existing fracture tips are 1.392×107 J/m^3, 2.433×10^7 J/m^3, and 4.248×10^7 J/m^3, respectively. The energy concentration area around the pre-existing fracture tips expands. In Figs. 12(b), 12(c) and 12(h), as the size of the pre-existing fracture increases, the gray area with an elastic strain energy density greater than 60,000 J/m^3 increases around the pre-existing fracture tips. These results demonstrate that as the size of the pre-existing fracture increases, the accumulated energy at the pre-existing fracture tips increases. The area with more strain energy is more likely to be damaged than an area with less energy. Hydraulic fractures are more likely to propagate towards areas with large strain energy. The

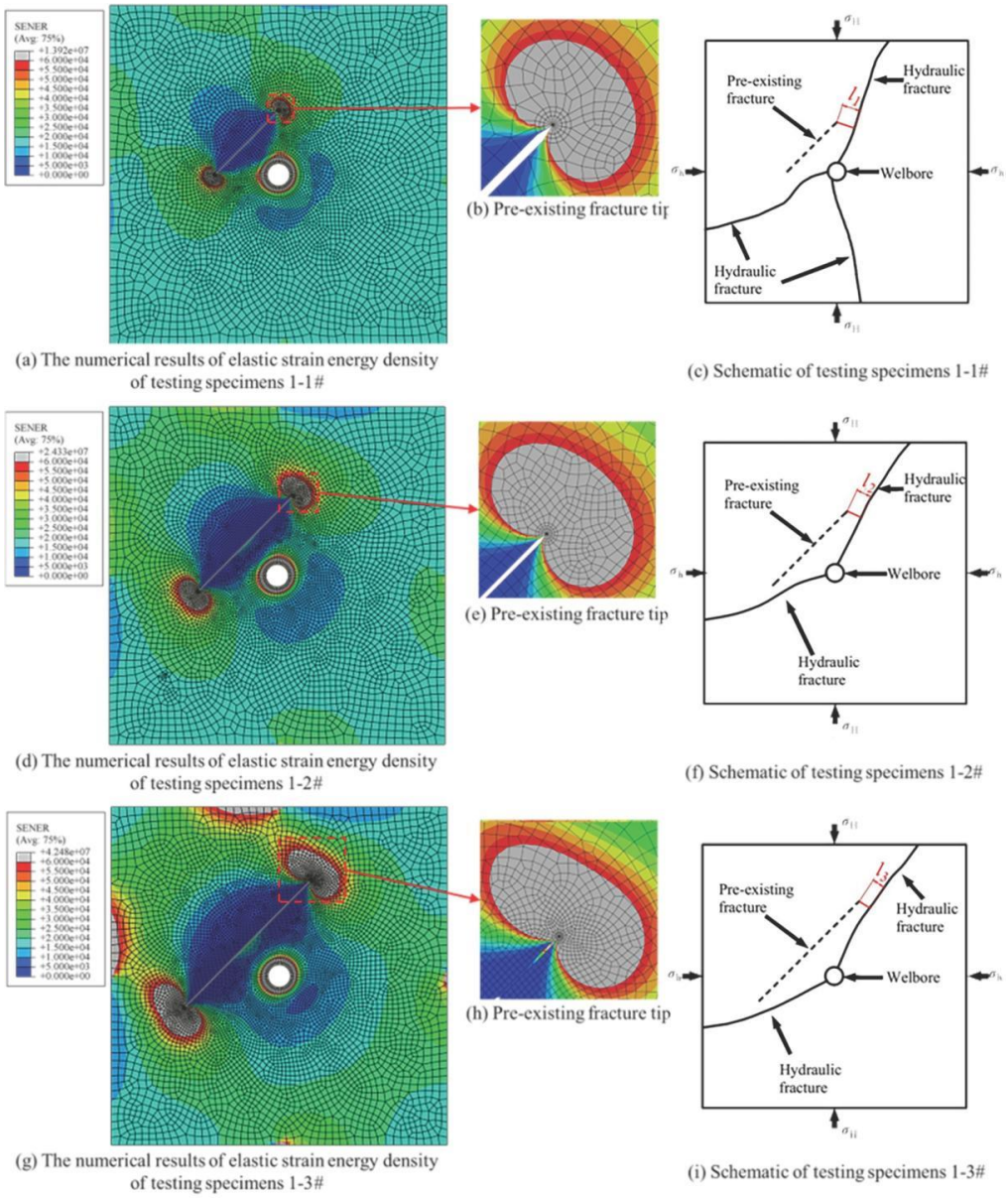

Fig. 12 The numerical results of elastic strain energy density of testing specimens 1-1#, 1-2#, 1-3#: (a), (d) and (e) are models of testing specimens 1-1#, 1-2# and 1-3#, respectively, (b), (e) and (h) are magnification pre-existing fracture tip locations of testing specimens 1-1#, 1-2# and 1-3#, respectively, (c), (f) and (i) are schematic diagrams of experimental results of 1-1#, 1-2# and 1-3#, respectively

larger the pre-existing fracture, the greater the energy near the pre-existing fracture tips, the stronger the attraction of the fracture tips to the hydraulic fracture. It can also be found from the experimental results that the distance between the hydraulic fracture and the pre-existing fracture tip decreases with increasing pre-existing fracture size, as shown in Figs. 12(c), 12(f), and 12(i). The numerical results are generally consistent with the experimental results.

During the propagation of hydraulic fractures, tensile stress concentration occurs near the pre-existing fracture tips, resulting in energy accumulation. The tensile stress magnitudes at the fracture tips vary with different pre-existing fracture sizes, as shown in Fig. 13. It is more difficult for strain energy to release in the compressive stress direction than in the tensile stress direction. As a result, hydraulic fracture is more easily to propagate towards the area with tensile stress concentration. When the stress states are the same, the probability of fracture propagation in the high strain energy area is higher than that in the low strain energy area.

Around the pre-existing fracture tips, induced stresses exist and are clearly concentrated. The propagation path of the hydraulic fracture is affected by the stress field at the pre-existing fracture tips. When the pre-existing fracture is short (40 mm), the maximum tensile stress near the pre-existing fracture tips is 0.029 MPa (Fig. 13(a)). As the size of the pre-existing fracture increases, the tensile stress near the fracture tips increases, and the maximum tensile stress reaches 0.838 MPa with a pre-existing fracture of 80 mm long, as shown in Fig. 13(c). With increasing pre-existing

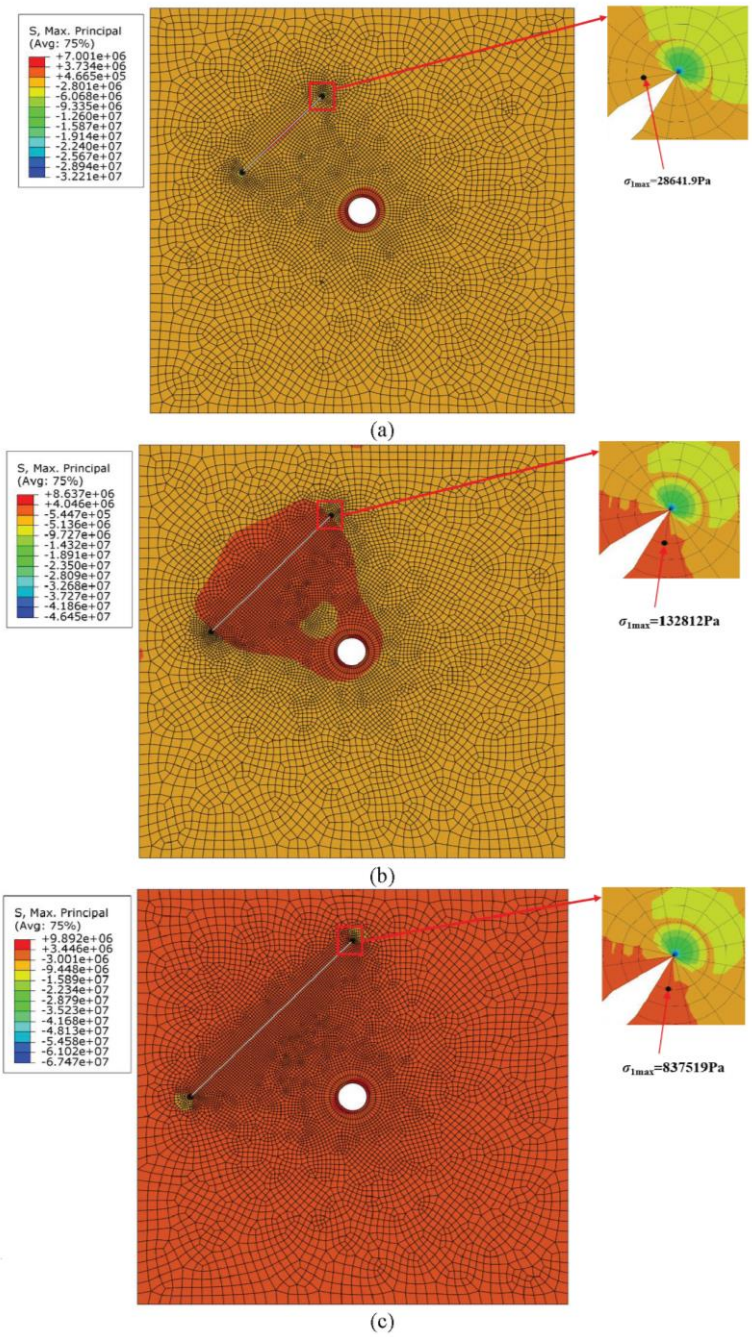

Fig. 13 The numerical results of maximum tensile stress at the fracture tips: (a), (b) and (c) are models of testing specimens 2-1#, 2-2# and 2-3#, respectively

fracture length, the tensile stress at the fracture tips increases, causing the hydraulic fracture to propagate towards the pre-existing fracture tips. .

We use the XFEM to simulate the hydraulic fracturing process affected by the pre-existing fracture, during which the fracture propagates towards the pre-existing fracture tips, and then rotates to the direction of the maximum principal stress. With increasing pre-existing fracture length, the distance between the hydraulic fracture and the pre-existing fracture tips decreases, indicating that the attraction effect of the pre-existing fracture on the hydraulic fracture increases with the pre-existing fracture length, as shown in Fig. 14.

To understand the effect of pre-existing fracture location on hydraulic fracturing, we use the finite element method to simulate the propagation process for specimens 1-1# and 3-1#. The pre-existing fractures are of the same size in specimens 1-1# and 3-1#. The distance between the pre-existing fracture and the wellbore in specimen 1-1# is shorter than that in specimen 3-1#. Fig. 15 shows the distribution of elastic strain energy density in these two specimens. As can be seen from Figs. 15(b) and 15(e), an energy concentration area appears around the wellbore after injection (the gray area with an elastic strain energy density greater than 60,000 J/m^3). The energy concentration area is affected by the pre-existing fracture position. As seen from

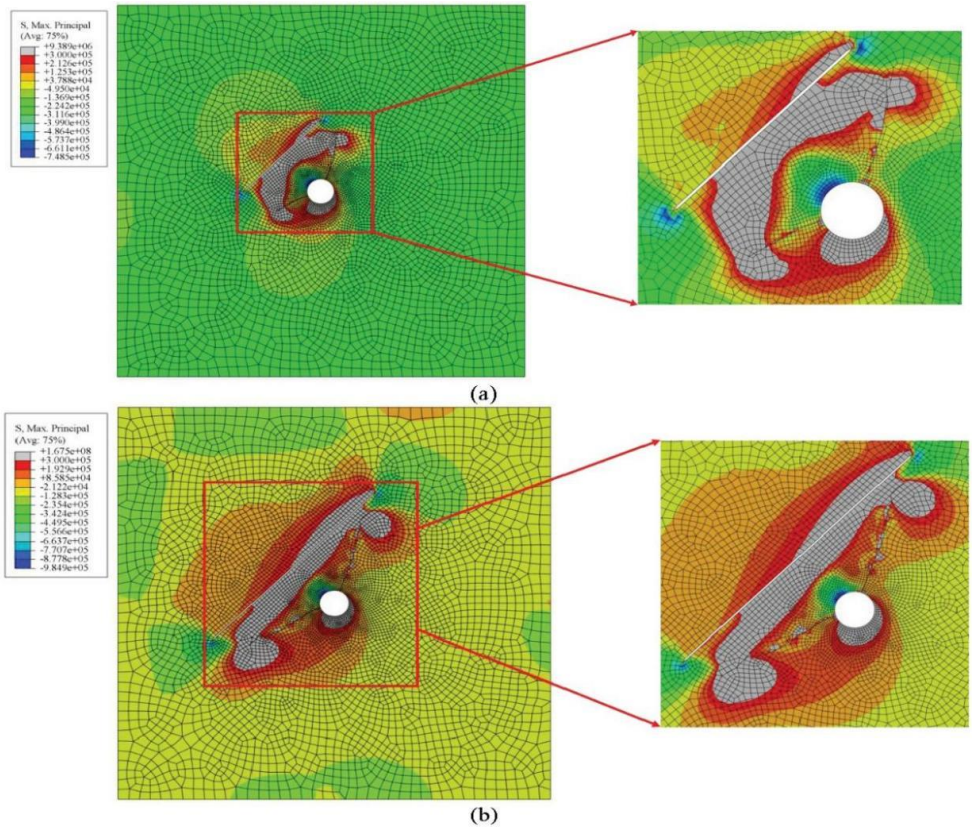

Fig. 14 Numerical simulation results of hydraulic fracture propagation (a) specimen 1-4# and (b) specimen 1-6#

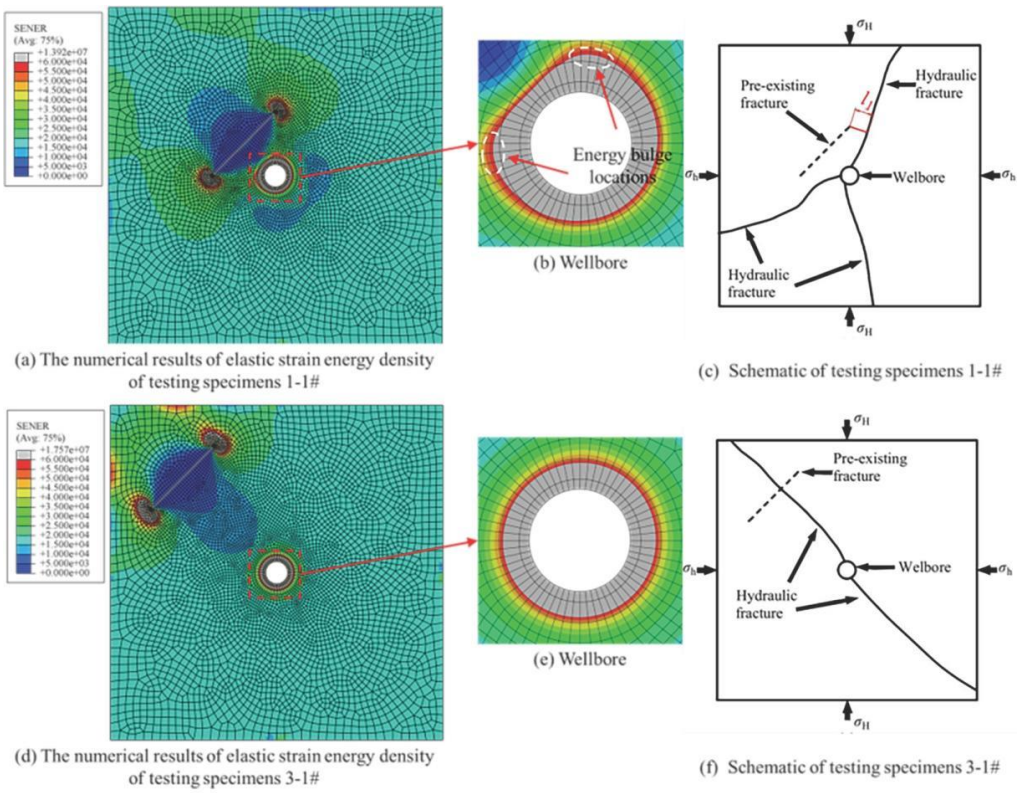

Fig. 15 The results of elastic strain energy density of testing specimens 1-1# and 3-1# were calculated by finite element method: (a) and (d) are testing specimens 1-1# and 3-1# respectively, (b) and (e) are magnification wellbore locations of testing specimens 1-1# and 3-1# respectively, (c) and (f) are schematic diagrams of experimental results of 1-1# and 3-1# respectively

Fig. 15(b), there are two bulge positions in the energy concentration area around the wellbore (indicated by the white dotted line). In addition, the closer the pre-existing fracture is to the wellbore, the more evident the energy bulge area around the wellbore becomes. Hydraulic fractures are initiated from these two energy bulge areas on the pre-existing fracture side of the wellbore in specimen 1-1#, as shown in Figs. 15(b) and 15(c). After initiation, hydraulic fractures are attracted by another energy concentration area (the pre-existing fracture tip area). When the pre-existing fracture is far away from the wellbore (specimen 3-1#, L=60 mm, L/D=6), the energy distribution around the wellbore is almost uniform and no significant energy bulge area exists, as shown in Fig. 15(e). In specimen 3-1#, there is only one initiation point on the pre-existing fracture side of the wellbore. After initiation, the hydraulic fracture propagates towards the middle of the pre-existing fracture rather than the tips. The attracting ability of pre-existing fracture tips in specimen 3-1# is smaller than that of specimen 1-1#. This indicates that with increasing distance between the pre-existing fracture and the wellbore, the impact of pre-existing fracture tips on hydraulic fracture propagation decreases.

5. Discussion

Numerous scholars have studied various factors affecting the propagation of hydraulic fractures. For instance, the conditions for hydraulic fractures to cross pre-existing fractures (natural fractures) is explored (Zhao *et al*. 2019, Liu *et al*. 2014, Cheng *et al*. 2014). Zhang *et al.* (2018) analyzed the effect of pre-existing fracture location on hydraulic fracture propagation behavior. In this study, we focused on the effect of pre-existing fracture size (length) (Figs. 3-8) that has received little attention to date. Experimental and numerical results in this work show that both pre-existing fracture size and distance between the wellbore and the pre-existing fracture influence the propagation of hydraulic fractures.

The numerical simulation results in Fig. 12 show that when the pre-existing fracture is very close to the wellbore (L/D=2 or 4), the elastic strain energy accumulated around the wellbore and the pre-existing fracture tips is larger than that at other locations (as shown in Figs. 12(a), 12(d) and 12(g)). Furthermore, the elastic strain energy density at the pre-existing fracture tips increases with increasing pre-existing fracture size. The energy distribution area around the wellbore also varies with the size of the pre-existing fracture. There may be two energy bulge positions in the energy concentration area around the wellbore when the pre-existing fracture is close to the wellbore (Fig. 15(b)). Hydraulic fracture propagation is affected by the surrounding energy field and fracture is more likely to propagate to the area with high strain energy. As a result, hydraulic fracture tends to initiate at an energy bulge area around the wellbore and propagates towards the pre-existing fracture tips.

With increasing distance between the wellbore and the pre-existing fracture, the attracting ability of the pre-existing fracture tips to hydraulic fractures is reduced. When the pre-existing fracture is far away from the wellbore (L/D=6), the energy distribution around the wellbore is almost uniform (Fig. 15(e)), and no obvious energy bulge area exists. The initiation and propagation of hydraulic fractures are more impacted by the pre-existing fracture rather than the tips. When the hydraulic fracture approaches the far away pre-existing fracture, even though attracting ability exsits, it could not overcome the propagation inertia towards the middle of the pre-existing fracture (Zhang *et al*. 2018). Therefore, when the pre-existing fracture is far away from the wellbore, the hydraulic fracture propagates towards the middle of the pre-existing fracture rather than the fracture tips.

6. Conclusions

In this work, we have conducted laboratory experiments and numerical simulations to investigate the role of pre-existing fracture size and position on hydraulic fracture propagation behavior. The following conclusions may be drawn from this study.

- For specimens in which the pre-existing fracture is relatively close to the wellbore (L/D=2, L/D=4), the size of the pre-existing fracture has an impact on hydraulic fracture propagation. The hydraulic fracture propagates towards the pre-existing fracture tips. The larger the pre-existing fracture size, the stronger attraction the pre-existing fracture tips have on the hydraulic fracture.
- With increasing distance between the wellbore and the pre-existing fracture, the attracting ability of the pre-existing fracture tips to the hydraulic fracture decreases.
- For specimens with the pre-existing fracture relatively far away from the wellbore (L/D=6), the pre-existing fracture size has limited impact on the attracting ability of pre-existing fracture tips to the hydraulic fracture. The hydraulic fracture propagates towards the middle of the pre-existing fracture rather than the fracture tips, independent of the pre-existing fracture length.

Acknowledgments

This paper is funded by the National Natural Science Foundation of China (NO. 51879151, 42272311), The Fundamental Research Funds of Shandong University No.2017JC001.

References

Al-Rubaie, A. and Mahmud, H. (2020), "A numerical investigation on the performance of hydraulic fracturing in naturally fractured gas reservoirs based on stimulated rock volume", *J. Petrol. Explor. Prod. Technol.*, **10**, 3333-3345. https://doi.org/10.1007/s13202-020-00980-8.

Behnia, M., Goshtasbi, K., Zhang, G. and Mirzeinaly Yazdi, S. (2015), "Numerical modeling of hydraulic fracture propagation and reorientation", *Eur. J. Environ. Civ. Eng.*, **19**(2), 152-167. https://doi.org/10.1080/19648189.2014.939306.

Bohloli, B. and de Pater, C.J. (2006), "Experimental study on hydraulic fracturing of soft rocks: Influence of fluid rheology and confining stress", *J. Petrol. Sci. Eng*., **53**, 1-12. https://doi.org/10.1016/j.petrol.2006.01.009.

Dai, C., Liu, H., Wang, Y., Li, X. and Wang, W. (2018), "A simulation approach for shale gas development in china with embedded discrete fracture modeling", *Mar. Petroleum Geol*., **100**, 519-529. https://doi.org/10.1016/j.marpetgeo.2018.09.028.

Dehghan, A.N., Goshtasbi, K., Ahangari, K. and Jin, Y. (2015), "Experimental investigation of hydraulic fracture propagation in fractured blocks", *B. Eng. Geol. Environ*., **74**, 887-895. https://doi.org/10.1007/s10064-015-0745-6.

Fan, T.G. and Zhang, G.Q. (2014), "Laboratory investigation of hydraulic fracture networks in formations with continuous orthogonal fractures", *Energy*, **74**, 164-173. https://doi.org/10.1016/j.energy.2014.05.037.

Guo, T.K., Zhang, S.C., Qu, Z.Q, Zhou, T., Xiao, Y.S. and Gao. J. (2014), "Experimental study of hydraulic fracturing for shale by stimulated reservoir volume", *Fuel*, **128**, 373-380. https://doi.org/10.1016/j.fuel.2014.03.029.

Hadei, M.R. and Veiskarami, A. (2021), "An experimental investigation of hydraulic fracturing of stratified rocks", *Bull. Eng. Geol. Environ*., **80**, 91-506. https://doi.org/10.1007/s10064-020-01938-0.

Ham, S.M. and Kwon, T.H. (2019), "Characteristics of steady-state propagation of hydraulic fractures in ductile elastic and two-dimensionally confined plate media", *Int. J. Rock Mech. Min. Sci*., **114**, 164-174. https://doi.org/10.1016/j.ijrmms.2018.12.023.

Hou, B., Zhang, R.X., Tan, P., Song, Y., Fu, W.N., Chang, Z., Kao, J.W., Muhadasi, Y. and Chen, M. (2018), "Characteristics of fracture propagation in compact limestone formation by hydraulic fracturing in central Sichuan", *J. Nat. Gas. Sci. Eng*., **57**, 122-134. https://doi.org/10.1016/j.jngse.2018.06.035.

Jang, Y. and Sung, W. (2015). "Modeling of multi-stage hydraulic fracture propagation", *J. Korean Inst. Gas*, **19**(5), 13-19. https://doi.org/10.7842/kigas.2015.19.5.13.

Jiang, T.T., Zhang, J.H., Huang, G., Song, S.X. and Wu, H. (2018), "Experimental study on the mechanical property of coal and its application", *Geomech. Eng*., **14**(1), 9-17. https://doi.org/10.12989/gae.2018.14.1.009.

Kwok, C.Y., Duan, K. and Pierce, M. (2020), "Modeling hydraulic fracturing in jointed shale formation with the use of fully coupled discrete element method", *Acta Geotech*., **15**, 245-264. https://doi.org/10.1007/s11440-019-00858-y.

Liu, Z.Y., Chen, M. and Zhang, G.Q. (2014), "Analysis of the influence of a natural fracture network on hydraulic fracture propagation in carbonate formations", *Rock Mech. Rock Eng*., **47**, 575-587. https://doi.org/10.1007/s00603-013-0414-7.

Luo, Z.F., Zhang, N.L., Zhao, L.Q., Yao, L.M. and Liu, F. (2018), "Seepage-stress coupling mechanism for intersections between hydraulic fractures and natural fractures", *J. Petrol. Sci. Eng*., **171**, 37-47. https://doi.org/10.1016/j.petrol.2018.07.019.

Nadimi, S., Miscovic, I. and McLennan, J. (2016), "A 3D peridynamic simulation of hydraulic fracture process in a heterogeneous medium", *J. Petrol. Sci. Eng*., **145**, 444-452. https://doi.org/10.1016/j.petrol.2016.05.032.

Salam, A.R. and Djebbar, T. (2013), "Pressure behaviours and flow regimes of a horizontal well with multiple inclined hydraulic fractures", *Int. J. Oil Gas Coal Technol.*, **6**, 207-241.

Taleghani, A.D., Gonzalez, M. and Shojaei, A. (2016), "Overview of numerical models for interactions between hydraulic fractures and natural fractures: Challenges and limitations", *Comput. Geotech.*, **71**, 361-368. https://doi.org/10.1016/j.compgeo.2015.09.009.

Tan, P., Jin, Y., Han, K., Hou, B., Chen, M., Guo, X.F. and Gao, J. (2017), "Analysis of hydraulic fracture initiation and vertical propagation behavior in laminated shale formation", *Fuel*, **206**, 482-493. https://doi.org/10.1016/j.fuel.2017.05.033.

Warpinski, N.R. and Teufel, L.W. (1984), "Influence of geologic discontinuities on hydraulic fracture propagation", *J. Petrol. Technol*., **39**(2), 209-220. https://doi.org/10.2118/13224-PA.

Wei, C., Zhang, B., Li, S.C., Fan, Z. and Li, C. (2021), "Interaction between hydraulic fracture and pre-existing fracture under pulse hydraulic fracturing", *SPE Production & Operations*, **36**(3), 553-571. https://doi.org/10.2118/205387-PA.

Yan, C., Ren, X., Cheng, Y., Zhao, K., Deng, F., Liang, Q., Zhang, J., Li, Y. and Li, Q. (2019), "An experimental study on the hydraulic fracturing of radial horizontal wells", *Geomech. Eng*., **17**(6), 535-541. https://doi.org/10.12989/gae.2019.17.6.535.

Zeng, X.G. and Wei, Y.J. (2017), "Crack deflection in brittle media with heterogeneous interfaces and its application in shale fracking", *J. Mech. Phys. Solid*., **101**, 235-249. https://doi.org/10.1016/j.jmps.2016.12.012.

Zhang, B., Liu, J.Y., Wang, S.G., Li, S.C., Yang, X., Li, Y., Zhu, P. and Yang, W. (2018), "Impact of the distance between pre-existing fracture and wellbore on hydraulic fracture propagation." *J. Nat. Gas. Sci. Eng.*, **57**, 155-165. https://doi.org/10.1016/j.jngse.2018.07.004.

Zhao, Y., He, P.F., Zhang, Y.F. and Wang, C. (2019), "A new criterion for a toughness-dominated hydraulic fracture crossing a natural frictional interface", *Rock Mech. Rock Eng.*, **52**(8), 2617-2629. https://doi.org/10.1007/s00603-018-1683-y.

JS